# The SNARE protein SNAP-25 is required for normal exocytosis at auditory hair cell ribbon synapses

Charlotte Calvet, Thibault Peineau, Najate Benamer, Maxence Cornille, Andrea Lelli, Baptiste Plion, Ghizlène Lahlou, Julia Fanchette, Sylvie Nouaille, Jacques Boutet de Monvel, et al.

iScience

CellPress
OPEN ACCESS

Article

# The SNARE protein SNAP-25 is required for normal exocytosis at auditory hair cell ribbon synapses

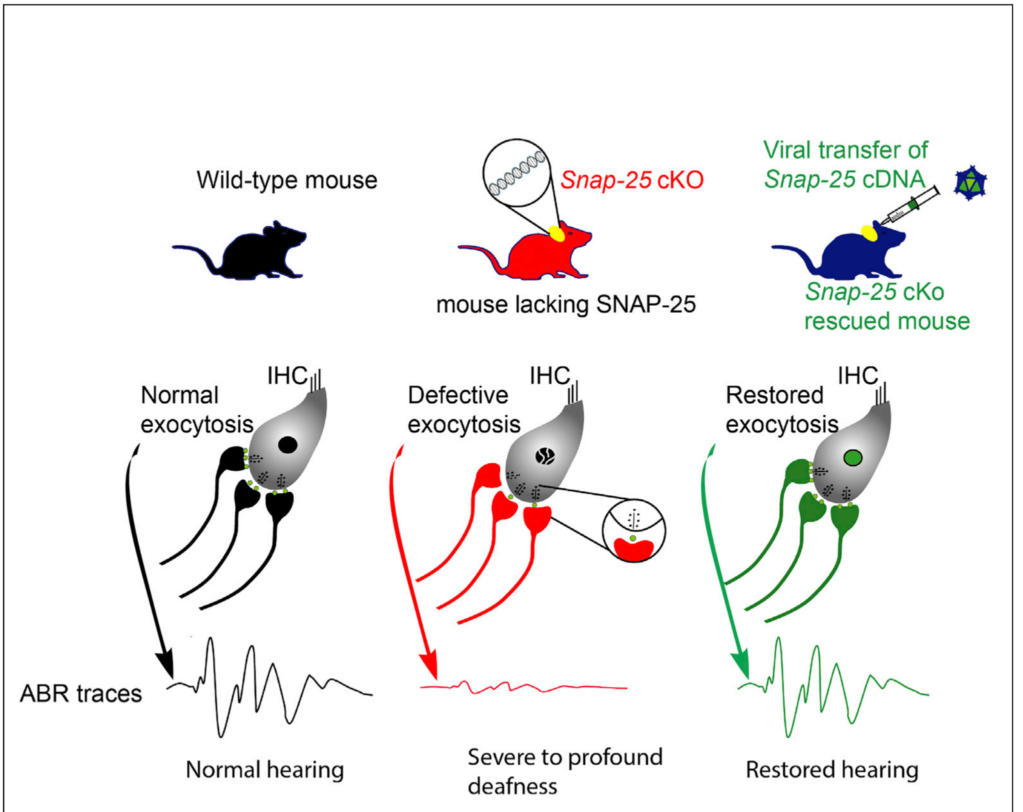


Charlotte Calvet, Thibault Peineau, Najate Benamer, ..., Christine Petit, Didier Dulon, Saaid Safieddine

saaid.safieddine@pasteur.fr

## Highlights

The inner hair cell (IHC), the genuine auditory sensory cell, expresses SNAP-25

IHC targeted deletion of SNAP-25 leads to deafness and synaptic degeneration

Without SNAP-25, the IHC transmitter release is drastically reduced

Viral transfer of SNAP-25 cDNA rescues hearing and prevents synaptic degeneration

Calvet et al., iScience 25, 105628
December 22, 2022 © 2022 The Authors.
https://doi.org/10.1016/j.isci.2022.105628

iScience

CellPress
OPEN ACCESS

Article

# The SNARE protein SNAP-25 is required for normal exocytosis at auditory hair cell ribbon synapses

Charlotte Calvet,[1,2] Thibault Peineau,[3] Najate Benamer,[1] Maxence Cornille,[1] Andrea Lelli,[1] Baptiste Plion,[1] Ghizlène Lahlou,[1,2,4] Julia Fanchette,[1,5] Sylvie Nouaille,[1] Jacques Boutet de Monvel,[1] Amrit Estivalet,[1] Philippe Jean,[1] Vincent Michel,[1] Martin Sachse,[6] Nicolas Michalski,[1] Paul Avan,[7] Christine Petit,[1] Didier Dulon,[1,3] and Saaid Safieddine[1,2,8,9,*]

## SUMMARY

**Hearing depends on fast and sustained calcium-dependent synaptic vesicle fusion at the ribbon synapses of cochlear inner hair cells (IHCs). The implication of the canonical neuronal SNARE complex in this exocytotic process has so far remained controversial. We investigated the role of SNAP-25, a key component of this complex, in hearing, by generating and analyzing a conditional knockout mouse model allowing a targeted postnatal deletion of *Snap-25* in IHCs. Mice subjected to IHC *Snap-25* inactivation after hearing onset developed severe to profound deafness because of defective IHC exocytosis followed by ribbon degeneration and IHC loss. Viral transfer of *Snap-25* in these mutant mice rescued their hearing function by restoring IHC exocytosis and preventing synapses and hair cells from degeneration. These results demonstrate that SNAP-25 is essential for normal hearing function, most likely by ensuring IHC exocytosis and ribbon synapse maintenance.**

## INTRODUCTION

The auditory sensory inner hair cells (IHCs) encode sound information into nerve impulses with high temporal precision and sensitivity over a wide range of stimulus intensities.[1–5] The depolarization of IHCs in response to sound-evoked deflection of their hair bundle results in rapid calcium influx through voltage-activated $Ca_v1.3$ $Ca^{2+}$ channels located in the IHC synaptic active zone,[6–8] and the subsequent binding of $Ca^{2+}$ ions to otoferlin, the calcium sensor controlling the fusion of IHC synaptic vesicles.[5,9–11] Striking functional and structural features of IHC synapses are the extremely fast and sustained vesicle exocytosis, and the presence of an electron-dense presynaptic organelle of submicron diameter called a ribbon, marking the center of the synaptic active zone. Each ribbon is surrounded by nearby synaptic vesicles some of which are tethered to it. Despite their functional and structural differences, IHC ribbon synapses and conventional central nervous system (CNS) synapses share key molecules of regulated $Ca^{2+}$-dependent synaptic vesicle exocytosis. IHC and CNS synapses are both equipped with the presynaptic scaffold proteins bassoon and RIM.[12,13] The presence of the neuronal SNARE (soluble N-ethylmaleimide sensitive factor attachment protein receptor) complex in auditory hair cell is well documented, including syntaxin 1, SNAP-25 and synaptobrevin1/2.[14–17] Although, these results led to the notion that vesicle fusion at CNS and IHC ribbon synapses involves similar SNARE proteins,[4,18,19] the study of null mutant mouse models failed to reveal a functional role for the neuronal SNARE proteins in IHC synaptic transmission.[14] This finding led to the proposal that the IHC synapses might operate without neuronal SNARE proteins.[14] However, existing null mutant mouse models for most of the neuronal SNARE proteins die at birth or shortly after.[20] Therefore, the IHC function in these mutants could only be analyzed indirectly using organotypic culture models, wherein the findings may not faithfully reproduce the *in vivo* functioning of IHC synapses in a healthy and mature hearing organ. To untangle this issue, we focused on SNAP-25, a key component of the canonical synaptic SNARE complex. We generated a hair cell-specific *Snap-25* conditional knockout (*Snap-25* cKO) mouse model to study the effect of acute inactivation of *Snap-25* in the IHCs, which turned out to cause deafness both when occurring at neonatal and at mature stages. We characterized these mice by *in vivo* auditory tests and *ex vivo* physiological (membrane capacitance) recordings, combined with imaging (immunostaining and transmission electron microscopy) experiments. We further performed a series of *in-vivo* rescue experiments by using viral-mediated transfer of *Snap-25* cDNA in the IHCs of the mutant mice. Our results demonstrate that SNAP-25 is essential for normal hearing function, most likely by ensuring IHC exocytosis and ribbon synapse maintenance.

[1]Institut de l'Audition, Institut Pasteur, INSERM, Université de Paris, 75012 Paris, France

[2]Sorbonne Université, Collège doctoral, 75005 Paris, France

[3]Bordeaux NeuroCampus, Université de Bordeaux, 33076 Bordeaux, France

[4]APHP, Sorbonne Université, Service d'ORL et de chirurgie cervico-faciale, 75013 Paris, France

[5]APHP, Service d'ORL et de chirurgie cervico-faciale, Hôpital Bichat - Claude-Bernard, 75018 Paris, France

[6]UTechS Ultrastructural Bio Imaging, Institut Pasteur, Université de Paris, 75015 Paris, France

[7]Laboratoire de Biophysique Sensorielle, Faculté de Médecine, Université; d'Auvergne, Biophysique Médicale, Centre Jean Perrin, 63000 Clermont-Ferrand, France

[8]Centre National de la Recherche Scientifique, France

[9]Lead contact

*Correspondence: saaid.safieddine@pasteur.fr

https://doi.org/10.1016/j.isci.2022.105628

## RESULTS

### Generation of mice with a hair cell-specific *Snap-25* inactivation

The expression of *Snap-25* in IHCs as well as its paralogs (*Snap-23*, *Snap-29*, *Snap-47*) were first confirmed using single-cell next generation sequencing of the transcriptome (Figure S1A and Table S1). Using multiplexed fluorescent *RNAscope* probes *in situ* hybridization (ISH) at single-cell resolution combined with hair cell immunomarker (see STAR methods), we were also able to specifically localize *Snap-25* mRNA to the auditory hair cells (Figure S1B). Of interest, the *Snap-25* mRNA puncta were highly enriched at the basolateral zone of the IHC where the ribbon synapses are located, suggesting a local protein production to meet the demand of IHC ribbon synapse activity[21] (Figure S1B). We then aimed to study the role of *Snap-25* in IHC function. To this end, we generated Snap-25lox/lox mice allowing a selective inactivation of Snap-25 in cochlear hair cells. In this mouse model, exon 4, which is common to the two SNAP-25 isoforms a and b, is flanked by two loxP sites that recombine in the presence of the Cre recombinase leading to the exon excision (Figure S2A). Snap-25 lox/lox mice were crossed with *PMyo15-hCre*$^{+/KI}$ mice, in which the expression of Cre recombinase, under the control of the myosin 15 promoter gene, was detected only in cochlear hair cells from postnatal day 1 (P1) onwards (Figure S2B).[22]

Specific primers were used to detect the wild-type allele, floxed, and deleted allele lacking *Snap-25* exon and to show the presence of the Myo15-cre allele and that the deletion of *Snap-25*'s exon 4 occurs only in the organ of Corti but not in tail biopsies (Figure S2A). Thus, in the cochlea of *Snap-25*$^{lox/lox}$/*PMyo15-hCre*$^{+/KI}$ mice, *Snap-25* inactivation occurs only in the auditory hair cells at early postnatal stages. We thereafter refer to these mice as *Snap-25* conditional knockout (*Snap-25* cKO) mice.

### *Snap-25* inactivation in neonatal mice leads to profound deafness

Unlike the *Snap-25* total knockout mice, which die at birth,[23] *Snap-25* cKO mice were viable and displayed a normal Mendelian pattern of inheritance. We first analyzed the morphoanatomy of the organs of Corti of these mice at various developmental stages, using myosin 6 as a marker of auditory hair cells (Figures 1A and 1B).[24] Up to P10, the organ of Corti of *Snap-25* cKO mice displayed near normal organization with three rows of OHCs and one row of IHCs (Figures 1A and 1B). However, at P10, digital image quantification of RNAscope ISH combined with hair cell marker showed that the IHCs of *Snap-25* cKO mice appeared ovoid in shape and underwent a strong reduction in *Snap-25* transcripts (10.21 $\pm$ 0.43 puncta; $n$= 47) in comparison to IHCs (20.78 $\pm$ 0.75 puncta, $n$ = 41) of wild-type mice (Figures 1C and S3). Similarly, the number of synaptic ribbons per IHC at P10, as counted in the mid-apical region of the cochlea, was significantly reduced in *Snap-25* cKO (9.6 $\pm$ 3.7, $n$ = 81 cells from 7 mice) compared to wild-type mice (22.6 $\pm$ 5.3, $n$ = 81 cells from 5 mice) (Mann-Whitney test, $p < 0.0001$) (Figure 1D). We then performed transmission electron microscopy (TEM) on ultrathin (60 nm) sections from P10 *Snap-25* cKO mice. Sections from the synaptic active zone of IHCs of these mice displayed a ribbon structure decorated with synaptic vesicles and facing the postsynaptic density of an auditory afferent dendrite (Figure 1E). From P10 onward though, the organ of Corti was found to undergo a rapid process of hair cell degeneration (Figures 1B and S4). The *Snap-25* cKO mice turned out to be profoundly deaf at adult stages, as shown by the absence of auditory brainstem responses (ABRs) to sounds at all frequencies tested and sound levels up to 110 dB SPL (Figure 1F).

### *Snap-25* inactivation in neonatal mice impairs IHC exocytosis

We next investigated the kinetics of IHC synaptic exocytosis in the mid-apical cochlear regions of *Snap-25* cKO mice before (P8) and at (P12) hearing onset, using membrane capacitance measurements performed *ex vivo* in microdissected organs of Corti (Figure 2). On P8, the level of exocytosis of the readily releasable pool of vesicles (RRP), recorded in response to short depolarizations ranging from 5 to 25 ms, was significantly reduced in IHCs of *Snap-25* cKO mice (Figures 2A and 2B; two-way ANOVA, $p < 0.05$) but sustained (slow) release (SRP) (i.e., for stimulations longer than 30 ms) was normal (two-way ANOVA, $p = 0.16$). IHCs from *Snap-25* cKO mice had normal size, as indicated by the value of their resting membrane capacitance (8.27 $\pm$ 0.33 pF, $n$ = 10), which did not differ significantly from the value measured in wild-type mice (9.03 $\pm$ 0.22 pF, $n$ = 7; unpaired-$t$ test, p = 0.1). The peak $Ca^{2+}$ currents amplitude and density ($Ca^{2+}$ current amplitude normalized by the IHC membrane capacitance) were not significantly affected (unpaired $t$ test, p = 0.05; p = 0.15, respectively Figure 2C). Of note, the mechanoelectrical transduction (MET) currents recorded by patch clamp on IHCs from P8 *Snap-25* cKO mice displayed amplitudes and kinetics similar to those of wild-type IHCs (Figure S5). On P12, both the fast (RRP) and the sustained (SRP) IHC exocytosis levels in *Snap-25* cKO mice were greatly reduced (two-way ANOVA, $p < 0.05$, Figure 2D). The IHC

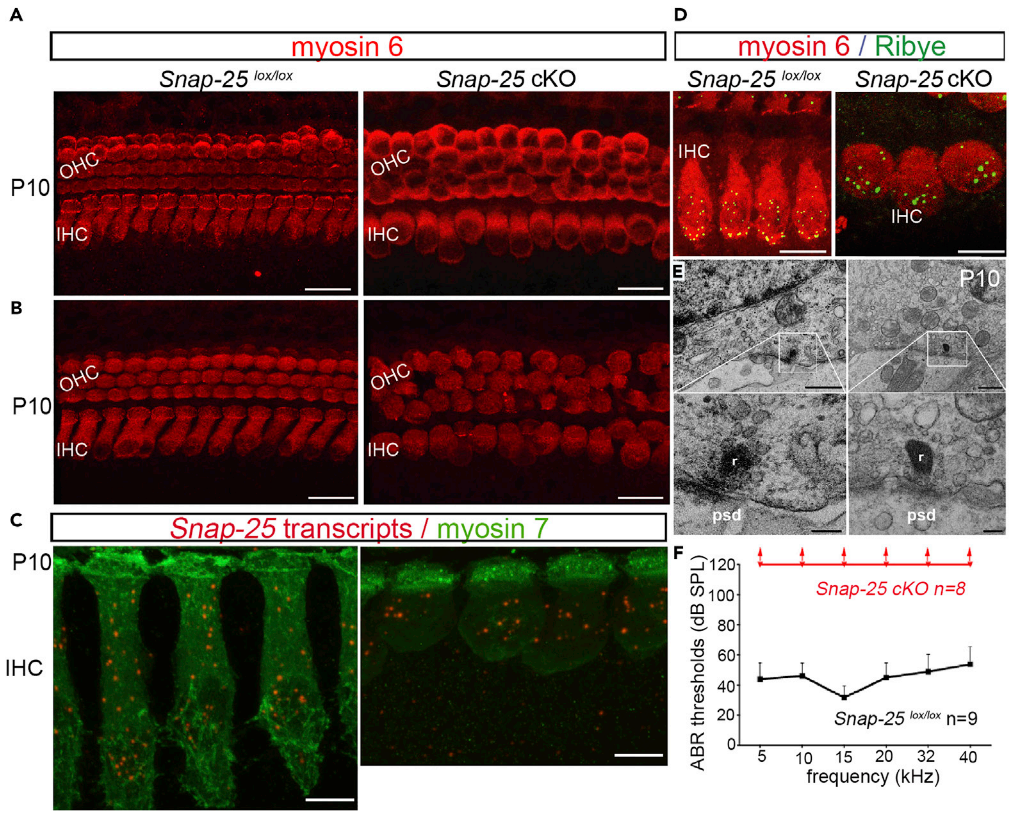


**Figure 1. Neonatal *Snap-25* deletion leads to profound deafness associated with ribbon degeneration and hair cell loss**

(A and B) Organs of Corti obtained on P8 (A) and P10 (B) from *Snap-25*$^{lox/lox}$ control (left), and *Snap-25* cKO (right) mice stained for the hair cell marker myosin 6 (red). Up to P10 the organ of Corti of *Snap-25* cKO mice displayed near normal organization with three rows of OHCs and one row of IHCs, Scale bars = 15 μm.

(C) Organs of Corti from *Snap-25*$^{lox/lox}$ control (left), and *Snap-25* cKO (right) subjected to *Snap-25* RNAScope ISH (red) and immunostained for myosin 7 (green), showing that the Snap-25 transcripts are severely reduced in the IHCs of the *Snap-25* cKO mice in comparison with the IHCs of the wild-type mice, scale bar (5 μm).

(D) P10 Organs of Corti from *Snap-25*$^{lox/lox}$ control and *Snap-25* cKO mice immunostained for myosin 6 (red) and the ribbon synapse presynaptic marker ribeye (green).

(E) 60 nm-thick transmission electron microscopy sections of IHC ribbon synapses from P10 *Snap-25*$^{lox/lox}$ control (left) and *Snap-25* cKO (right) mice. The insets at higher magnification show that, in both genotypes, the synapses contain a ribbon (r) decorated with synaptic vesicles facing the postsynaptic density (psd) of a primary auditory dendrite. Upper and lower Scale bars are 100 nm and 500 nm, respectively.

(F) Auditory brainstem responses recorded in *Snap-25* cKO mice ($n$ = 8) and *Snap-25*$^{lox/lox}$ control mice (n = 9) on P30.

resting membrane capacitance was reduced by almost half, from 10.89 ± 0.73 pF in wild-type mice ($n$ = 11) to 5.85 ± 0.62 pF in mutant mice ($n$ = 6) (unpaired $t$ test p< 0.01), suggesting imbalance of IHC plasma membrane recycling process during early stage of hair cell development which is in agreement with previous observations in cultured neurons lacking *Snap-25*.[25] The amplitude of total IHC $Ca^{2+}$ currents was also halved (unpaired $t$ test p = 0.001), but the total $Ca^{2+}$ current to membrane capacitance ratio remained unchanged (unpaired $t$ test, p = 0.24, Figures 2E and 2F). Altogether, these results suggest that SNAP-25 is required for recycling process of the plasma membrane and for exocytosis at immature IHC ribbon synapses.

## *Snap-25* inactivation after the hearing onset causes deafness in *Snap-25*$^{lox/lox}$ mice by impairing IHC exocytosis

The cochlea of *Snap-25* cKO mice, wherein the inactivation of *Snap-25* occurs at neonatal stages, undergoes a rapid degeneration of the auditory hair cells starting at about the onset of hearing (i.e. P12), excluding any further investigation of hearing in adult mice. To establish the function of SNAP-25 in mature IHCs, the Cre

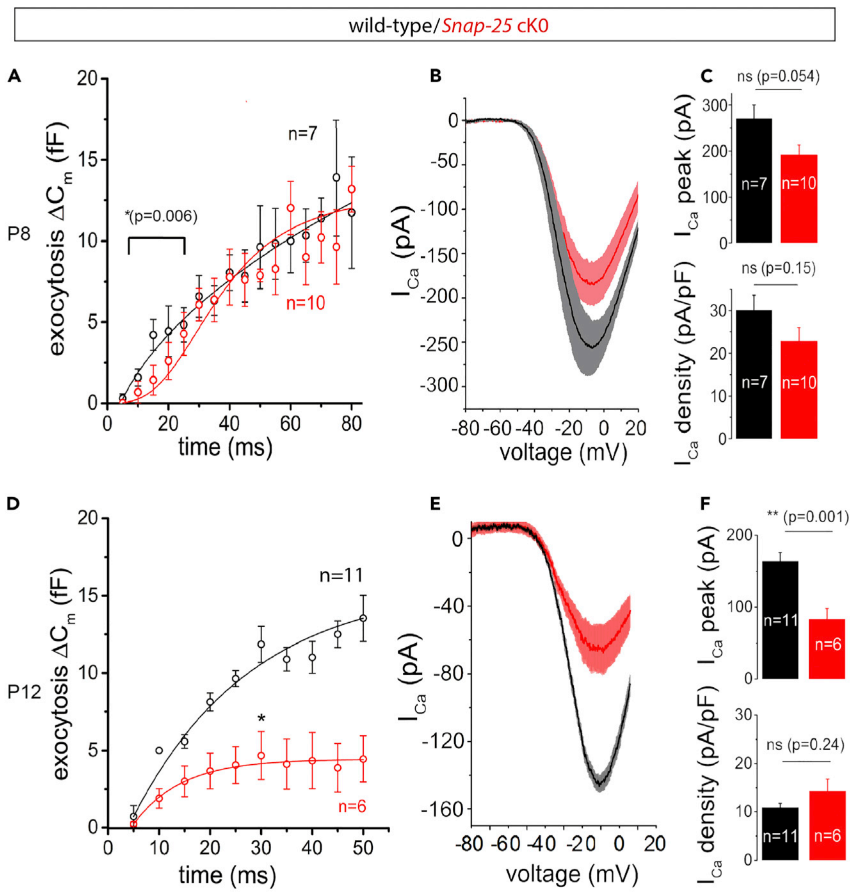


**Figure 2. Neonatal *Snap-25* inactivation disrupts IHC $Ca^{2+}$-evoked exocytosis**

(A) Kinetics of IHC exocytosis in *Snap-25$^{lox/lox}$* control and *Snap-25* cKO P8 mice evoked during various voltage-steps of increasing duration from −80 mV to −10 mV.

(B) $Ca^{2+}$ currents evoked by a voltage-ramp protocol (1 mV/ms from −90 to +30 mV) in *Snap-25$^{lox/lox}$* control and *Snap-25* cKO P8 mice.

(C) Peak $Ca^{2+}$ current amplitude (top) and $Ca^{2+}$ current density (bottom) in P8 *Snap-25* cKO mutant and *Snap-25$^{lox/lox}$* control IHCs.

(D) Kinetics of IHC exocytosis in *Snap-25$^{lox/lox}$* control and *Snap*-25 cKO mice on P12.

(E) $Ca^{2+}$ currents evoked by a voltage-ramp protocol (1 mV/ms from −90 to +30 mV) in *Snap-25$^{lox/lox}$* control and *Snap*-25 cKO mice on P12

(F) Peak $Ca^{2+}$ current amplitude (at top) and $Ca^{2+}$ current density (at bottom) in P12 in *Snap-25 $^{lox/lox}$* control and *Snap-25* cKO mice.

enzyme was delivered to mature IHCs using the Cre-recombinase-expressing AAV vector (AAV8-GFP-Cre) that was injected into the cochlea of *Snap-25$^{lox/lox}$* mice on P14 (i.e. after hearing onset). We first analyzed the cellular tropism and innocuity of AAV8-GFP-Cre in the mature cochlea of wild-type mice. Following the injection of AAV8-GFP-Cre into the cochlea of P14 mice, the organ of Corti was microdissected on P30 and immunostained for myosin 6 and GFP-Cre. We found that AAV8-GFP-Cre transduced almost all the IHCs throughout the entire cochlear spiral with no hair cell loss (Figure 3A). In these control mice, no significant effects could be detected on ABR thresholds which remained normal and like those measured in non-injected P30 wild-type mice, except at 15 kHz, for which a small elevation of about 5 dB was noticed (Figure 3B). By contrast, *Snap-25$^{lox/lox}$* mice ($n$ = 14) subjected to Cre-mediated *Snap-25* inactivation on P14 displayed a progressive but significant increase in ABR thresholds from P22 onward (Figures 3C–3E). On P30, the increase in ABR thresholds relative to non-injected *Snap-25$^{lox/lox}$* mice (n = 16) ranged from 20 to 40dBat all sound frequencies tested (5, 10, 15, 20, 32, and 40 kHz; unpaired $t$ tests, p< 0.001; <0.01; <0.001; <0.01; <0.001; <0.001, respectively; Figure 3D). Ten to twelve weeks after *Snap-25* inactivation, the ABR thresholds exceeded 75 dB SPL at all frequencies tested, indicating severe to profound deafness

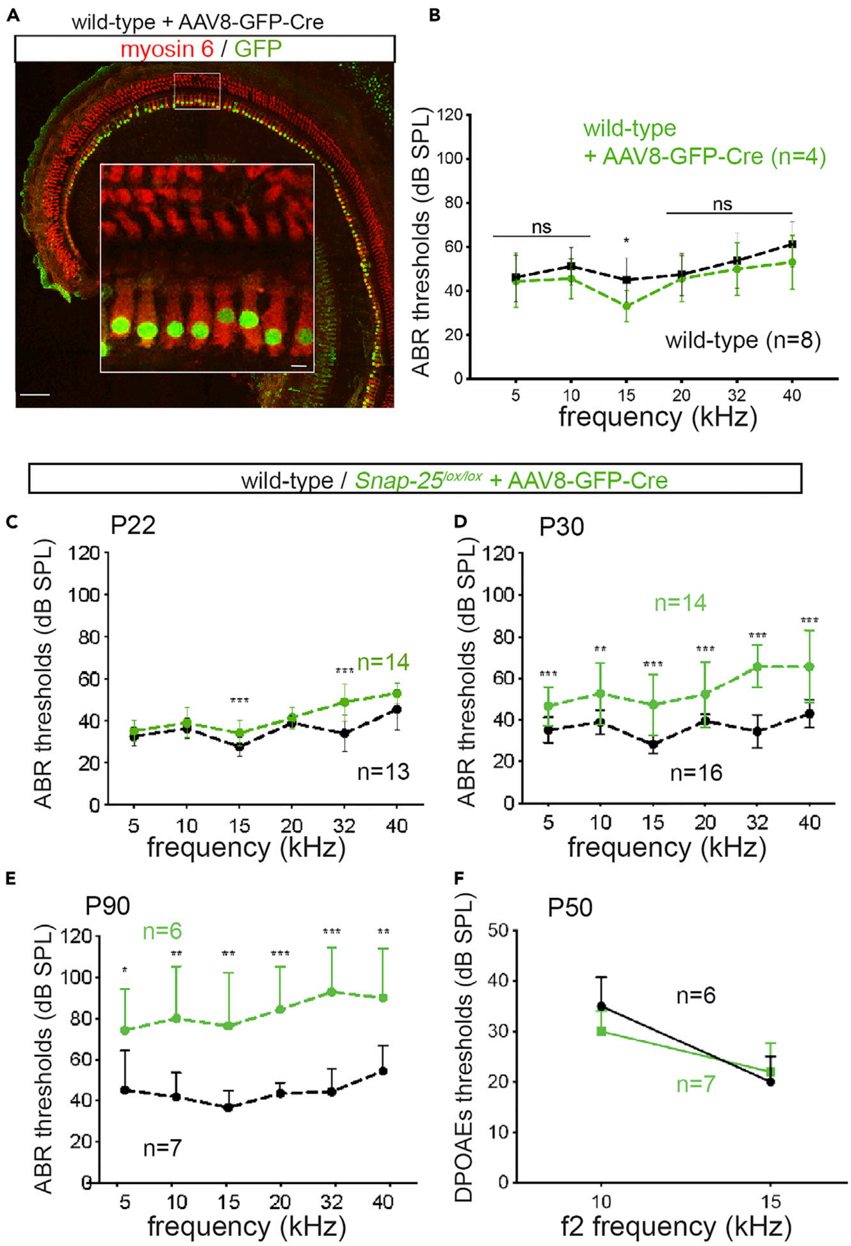


**Figure 3. *Snap-25* deletion in hearing mice leads to progressive deafness**

(A) Organ of Corti from the mid-to-apical turn of the cochlea of a P30 wild-type mouse injected with AAV8-GFP-Cre on P14 and immunostained for myosin 6 (red) and GFP-Cre (green). The inset shows a high magnification of the IHCs of the middle turn of the cochlea. Scale bars: 10 μm inset and 100 μm in overview.

(B) ABR thresholds were recorded at P20-P25 in wild-type mice after injection of AAV8-GFP-Cre on P14 (green) and in non-injected wild-type control mice (black).

(C–E) ABR thresholds recorded in P22 (C), P30 (D) and in P90 (E) Snap-*25$^{lox/lox}$* mice injected on P14 with AAV8-GFP-Cre (green) and *Snap-25$^{lox/lox}$* control mice (black).

(F) DPOAE recorded in P50 *Snap-25$^{lox/lox}$* mice injected on P14 with AAV8-GFP-Cre (green) and in Snap-*25$^{lox/lox}$* control mice (black).

(t tests, $p < 0.05$; <0.01; <0.01; <0.001; <0.001; <0.01, respectively, $n = 6$ injected *Snap-25$^{lox/lox}$* mice, $n = 7$ wild-type mice) (Figure 3E). The amplitude of ABR wave I, which reflects the synchronous firing of the primary auditory neurons as a function of sound intensity, when measured at 10 kHz and 80 dB SPL, was significantly reduced in mice subjected to intracochlear Cre injection (0.40 ± 0.03 μV, $n = 39$ mice, measured at 10 kHz and 80 dB SPL) compared to non-injected *Snap-25*$^{lox/lox}$ mice (0.83 ± 0.03 μV, *n* = 6 mice) (Mann-Whitney test, p < 0.001). In contrast, distortion product otoacoustic emissions (DPOAEs), which probe the functional integrity of OHCs, remained unaffected until P50, the last time point tested (Mann-Whitney test, p > 0.99, *n* = 6 *Snap-25*$^{lox/lox}$ injected mice, *n* = 7 wild-type mice), suggesting that the inactivation of *Snap-25* after hearing onset did not impair the cochlear amplifier function of the OHCs (Figure 3F). The observed increase in ABR thresholds with a decrease in wave I amplitude, and normal DPOAEs, is indicative of an auditory neuropathy or synaptopathy in *Snap-25*$^{lox/lox}$ mice subjected to Cre-mediated *Snap-25* inactivation, likely arising from a functional defect of the IHC ribbon synapses. Indeed, recordings of $Ca^{2+}$-evoked exocytosis in Cre-positive IHCs from AAV8-GFP-Cre-injected ears of *Snap-25*$^{lox/lox}$ mice on P30 revealed a significant decrease in the fast exocytotic release component (p< 0.05; two-way ANOVA) despite normal $Ca^{2+}$ currents (peak amplitude comparison, unpaired *t* test, p = 0.19) (Figures 4A and 4B). The $Ca^{2+}$ efficiency of exocytosis was also strongly reduced for a short 10 ms depolarization (unpaired *t* test, p< 0.001) but not for a long 70 ms depolarization (Figure 4C), indicating an abnormal fusion of IHC synaptic vesicles belonging to the RRP. The slow component of exocytosis, reflecting synaptic vesicle recruitment on repeated stimulation longer than 50 ms, was however unaffected (unpaired *t* test, p = 0.38) (Figure 4D), suggesting the SRP exocytosis is supported by a residual pool of the SNAP-25 protein and/or redundant SNAP-25 homologs, which are also present in IHCs (Figure S1A).[19] The impairment of the RRP response in IHCs lacking *Snap-25* was further confirmed in $Ca^{2+}$ uncaging experiments, which directly probe the function of the synaptic machinery independently of voltage-triggered $Ca^{2+}$ currents (Figure 4E). In P30 IHCs from AAV8-GFP-Cre-injected mice, intracellular $Ca^{2+}$ uncaging evoked maximal levels of exocytosis responses similar to those of IHCs from control (non-injected) *Snap-25*$^{lox/lox}$ mice (1.18 ± 0.15 pF, *n* = 13, and 1.16 ± 0.13 pF, *n* = 13, respectively, unpaired *t* test, p = 0.49), indicating that the total number of competent synaptic vesicles for fusion was unaffected in IHCs lacking *Snap-25* (Figure 4E). The maximal rate of exocytosis in IHCs from AAV8-GFP-Cre-injected mice (32.5 ± 1.18 fF/ms (*n* = 13)) was also similar to that measured in control IHCs (32.7 ± 2.1 fF/ms (*n* = 13), unpaired *t* test, p = 0.36) (Figure 4F). However, the onset of exocytosis in IHCs from AAV8-Cre-injected mice was largely delayed (Figures 4F and 4G) (latencies of 22.2 ± 3.7 ms in injected versus 8.5 ± 1.30 ms in injected versus non-injected mice, respectively, n = 13 mice in both cases, unpaired *t* test, p< 0.01). The deafness observed in mice subjected to *Snap-25* inactivation after the onset of hearing thus appeared to be due to an increased latency of RRP release. This finding is in line with previous reports demonstrating that SNAP-25 is critical for the fast component of exocytosis.[26] We then performed quantitative analyses of the number of ribbon synapses per IHC in the *Snap-25*$^{lox/lox}$ mice that underwent AAV8-GFP-Cre-injection at mature stages. Two weeks after Cre delivery (P28-P30), a stage on which synaptic exocytosis was probed, the organ of Corti of the injected *Snap-25*$^{lox/lox}$ mice were microdissected and immunolabeled for otoferlin, Ribeye and GluA2 (Figure 4H). We found that the number of synapses per IHC was significantly smaller in the Cre-positive cells (9.1 ± 4.9 *n* = 53 cells from 7 mice) than in wild-type IHCs (17.7 ± 1.5 *n* = 66 cells from 6 mice; Mann-Whitney test, p< 0.0001). In addition, throughout the cochlear spiral cochlea at this stage, we observed the presence of patches of immunostained IHCs separated by zones devoid of IHC, that had considerably expanded by the age of three months (Figure S6).

Together, our results suggest that the inactivation of *Snap-25* expression in these normally hearing mice impaired mainly the fast component of IHC exocytosis causing the degeneration of ribbon synapses and subsequently that of IHCs. This hypothesis is consistent with the notion that synaptic dysfunction contributes first to pathogenic progression of noise or aging-induced hearing loss before the occurrence of neuronal and hair cell degeneration.[27–30]

### *In vivo* gene replacement rescues hearing and IHC exocytosis in *Snap-25* cKO mice

To verify that the defects described above were caused specifically by the conditional inactivation of *Snap-25*, we carried out rescue experiments through a gene replacement strategy. We used an AAV viral vector expressing *Snap-25* previously shown to rescue neuroexocytosis in embryonic chromaffin cells of *Snap-25* null mice.[31] Viral vector expressing *Snap*-25 driven by the CMV promoter were delivered to the cochlea of *Snap-25* cKO mice on P2. Remarkably, ABR recordings showed that, unlike untreated *Snap-25* cKO mice, the rescued mice had sizeable ABRs three weeks after *Snap-25* cDNA transfer, with auditory thresholds ranging from wild-type levels to 30–40 dB above those levels (Figure 5A). The mean amplitude of wave I at 80 dB SPL in response to 10 kHz tone bursts was also significantly rescued in *Snap-25* cKO treated mice (0.45 μV ± 0.020, *n* = 7) compared to non-treated mice (not detectable), reaching about half of that in wild-type control mice at 10 kHz (0.93μV ± 0.04, *n* = 9, *t* test, p< 0.05). The number of synaptic ribbons per IHC in rescued mice (13.4 ± 3.2, *n* = 25 cells from 3 mice) was significantly higher than that of IHCs

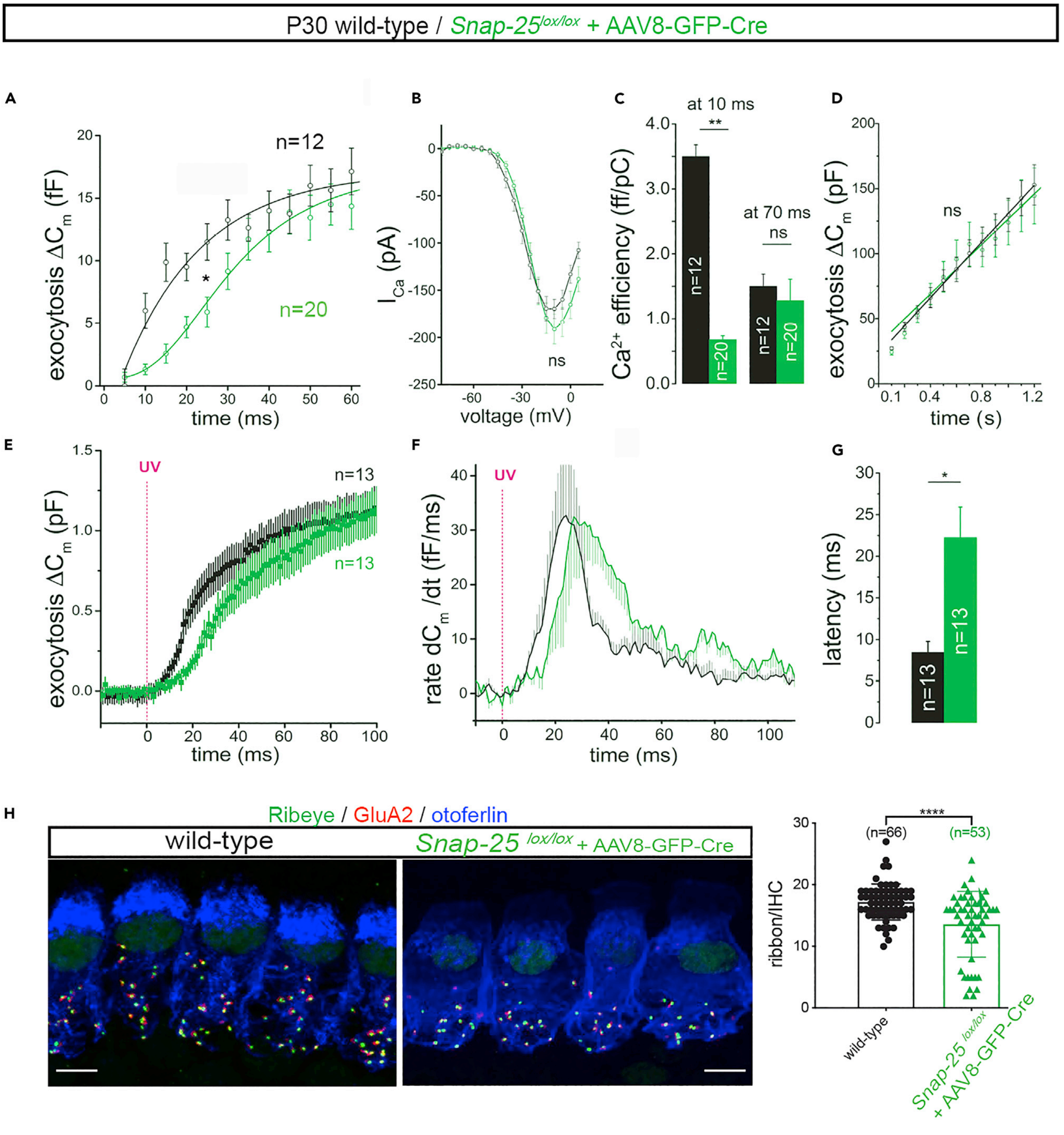


**Figure 4. *Snap-25* deletion in hearing mice disrupts fast exocytosis**

(A–D) IHC electrophysiological parameters assessed on P28-P30 *Snap-25* $^{lox/lox}$ mice having received AAV8-GFP-Cre injection on P14 (green) and *Snap-25*$^{lox/lox}$ control mice (black). (A) Kinetics of IHC exocytosis for brief depolarizing steps (from −80 to −10 mV). (B) $Ca^{2+}$ current amplitude as a function of IHC depolarization. (C) Exocytotic $Ca^{2+}$ efficiency measured for a 10 ms or a 70 ms voltage depolarization. (D) Mean cumulative ΔCm responses from GFP-positive and control IHCs elicited with 100 ms repetitive voltage steps from −80 mV to −10 mV.

(E) Exocytosis evoked by $Ca^{2+}$ uncaging, maximum release rate (F) and latency of exocytosis onset.

(G) in *Snap-25* cKO mice having received AAV8-*Snap-25*-injection and *Snap-25*$^{lox/lox}$ control mice.

(H) Maximum-intensity projections of confocal z-sections of IHCs from the cochlear middle turn of a *Snap-25*$^{lox/lox}$ control (left) and Cre injected *Snap-25*$^{lox/lox}$ (middle) mouse, immunostained for ribeye (green), GluA2 (red) and otoferlin (blue) at P30. Right, number of synaptic ribbons per IHC of *Snap-25*$^{lox/lox}$ control and of *Snap-25*$^{lox/lox}$ mice subjected to *Snap-25* inactivation on P14.

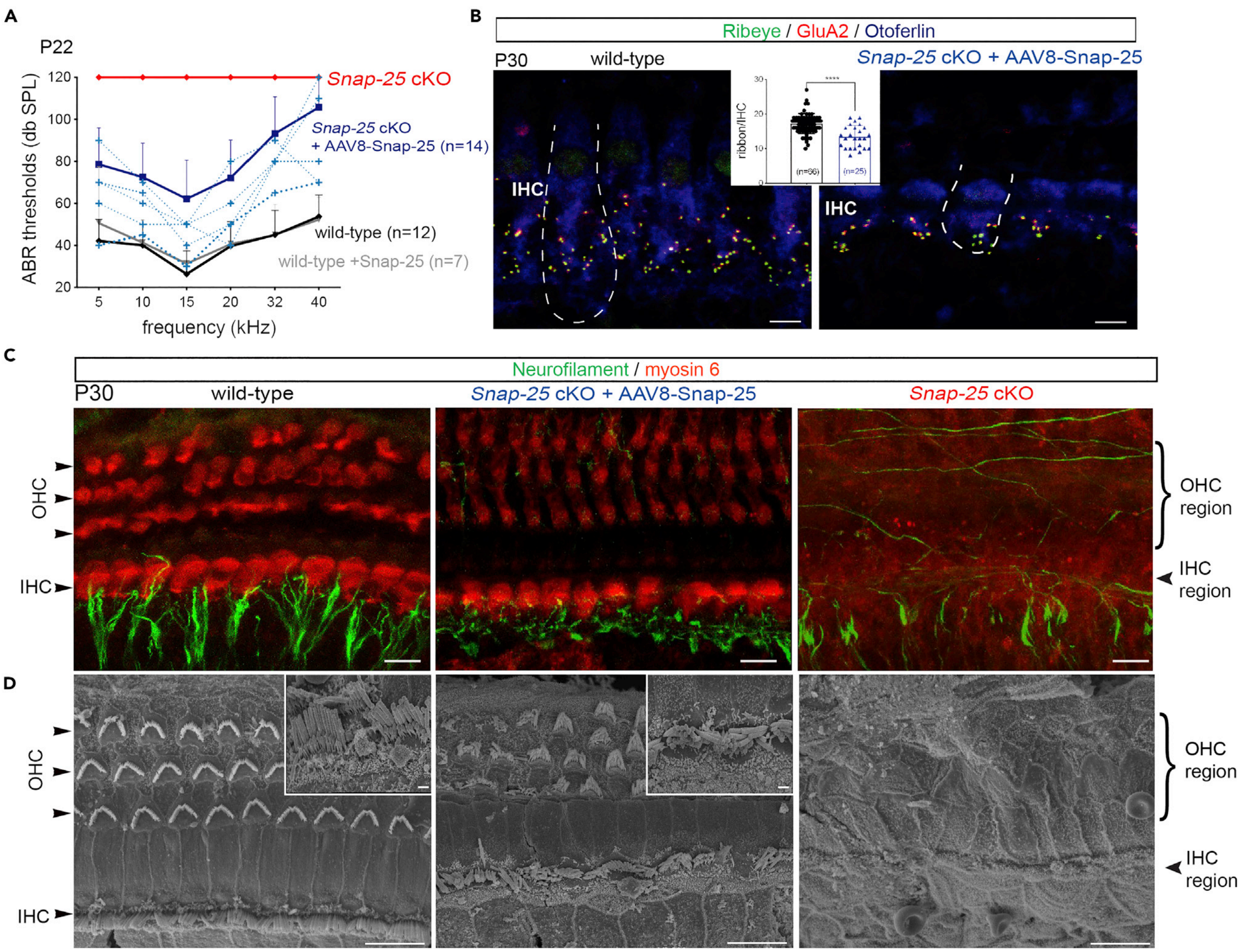


**Figure 5. *In vivo* gene replacement rescues hearing and prevents IHC loss in *Snap-25* cKO mice**

(A) ABR thresholds recorded between P20 and P25 in *Snap-25* cKO mice (red), *Snap-25* cKO mice rescued with AAV8-*Snap-25* on P2 (blue), *Snap-25*$^{lox/lox}$ control mice (black) and *Snap-25*$^{lox/lox}$ control mice injected with AAV8-*Snap-25* on P2 (gray). Hearing thresholds were significantly improved in *Snap-25* cKO rescued mice. The five *Snap-25* cKO mice for which rescue was most effective are represented by blue dotted curves.

(B) Maximum-intensity projections of confocal z-sections of IHCs from the cochlear middle turn of a *Snap-25*$^{lox/lox}$ control (at left) and rescued (at right) mouse, immunostained for ribeye (green), GluA2 (red) and otoferlin (blue) on P30. Scale bars = 5 μm, dotted line outline two IHCs. Inset is a bar charts showing the number of synaptic ribbons per IHC in P30 *Snap-25*$^{lox/lox}$ control and rescued *Snap-25* cKO mice.

(C) Maximum-intensity projections of confocal z-sections from the cochlear middle turn of a *Snap-25*$^{lox/lox}$ mouse (at left), a *Snap-25* cKO mouse rescued with the AAV8-*Snap-25* cDNA at P2 (at middle) and a *Snap-25* cKO mouse (at right), immunostained at P30 for myosin 6 (red) and neurofilament (green), to identify hair cells and auditory afferent fibers, respectively. Note the complete loss of hair cells in the *Snap-25* cKO mice compared to the AAV8-*Snap-25* rescued mice. Scale bar = 5 μm.

(D) Intermediate - and high-magnification scanning electron micrographs of the apical surface of the middle turn of P30 organs of Corti from a control *Snap-25*$^{lox/lox}$ control mouse (left), a *Snap-25* cKO mouse rescued on P2 (middle), and a non-rescued *Snap-25* cKO mouse (right); scale bars are 1 μm and 10 μm for inset and overview, respectively.

from mice subjected to *Snap-25* inactivation (9.1 ± 4.9 $n$ = 53 cells from 7 mice; unpaired $t$ test, p< 0.001), but remained lower than that of wild-type IHCs (17.3 ± 2.6, $n$ = 25 cells from 3 mice unpaired $t$ test, p< 0.0001) (Figure 5B), potentially accounting for the incomplete recovery of the ABR wave I amplitude in rescued *Snap-25* cKO mice. Consistent with these findings, whole-mount preparations of the organ of Corti immunolabeled for myosin 6 and neurofilament to identify hair cells and auditory afferent fibers, respectively, confirmed the complete loss of hair cells in the *Snap-25* cKO mice and no IHC degeneration had occurred up to P30 in the rescued mice, and that afferent innervation was preserved throughout the entire cochlea ($n$ = 171 cells from 5 mice) (Figure 5C). Furthermore, scanning electron microscopy analyses of the organs of Corti showed a near complete loss of both OHCs and IHCs in non-rescued *Snap-25* cKO mice on

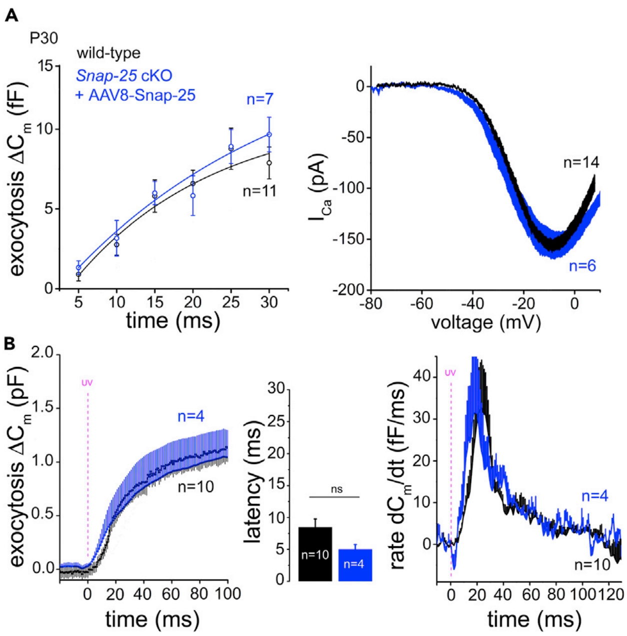


**Figure 6. *In vivo* gene replacement rescues IHC exocytosis in *Snap-25* cKO mice**

(A) RRP exocytosis (left) and calcium currents (right) recorded in IHCs from P30 *Snap-25* cKO mice rescued on P2 (blue curve) and *Snap-25*$^{lox/lox}$ control mice (black curve).

(B) Exocytosis evoked by $Ca^{2+}$ uncaging (left), latency of exocytosis onset (middle) and maximum release rate (right) in *Snap-25* cKO mice having received AAV8-*Snap-25*-injection and *Snap-25*$^{lox/lox}$ control mice.

P30 (Figure 5D). By contrast, the rescued mice had well-preserved organs of Corti at that stage, with a morpho-structural organization of IHCs and OHCs similar to that of wild-type hair cells (Figure 5D). To verify that the restoration of auditory function was associated with a rescue of the IHC exocytotic function, we monitored $Ca^{+}$-evoked exocytosis in IHCs from AAV-rescued *Snap-25* cKO mice at 4 weeks of age. Upon voltage-step depolarization, exocytosis and calcium currents recorded in IHCs from P30 *Snap-25* cKO mice injected with AAV8-Snap-25 on P2 were similar to those from wild-type mice (similar fast exocytosis kinetics, two-way ANOVA, p = 0.10, and similar $I_{Ca}$ peak amplitudes, unpaired *t* test, p = 0.34; Figure 6A). $Ca^{2+}$ uncaging experiments further confirmed that RRP exocytosis kinetics in transduced IHCs were also restored to wild-type levels including maximal ΔCm (1.5 ± 0.1 pF (*n* = 4) and 1.8 ± 0.2 pF (*n* = 10), respectively; unpaired t-test; p = 0.9) with a similar maximal rate of exocytosis (31 ± 10 fF/ms and 33 ± 5 fF/ms, respectively; unpaired *t*-test, p= 0.2), and a similar onset latency (5.0 ± 0.5 ms (*n* = 4) and 8.5 ± 1.3 ms, respectively, (*n* = 10); unpaired *t* test, p = 0.17; Figure 6B).

Overall, these data demonstrated that intracochlear AAV-mediated *Snap-25* delivery effectively rescued IHC exocytosis and hearing in *Snap-25* cKO mice.

## DISCUSSION

Since their discovery, overwhelming evidence has accumulated that the neuronal SNAREs syntaxin 1, SNAP-25, and synaptobrevin1/2[32,33] are essential for fast neurotransmitter release and for neuropeptide secretion.[23,34–41] However, because of the lack of appropriate animal models, the role of these neuronal SNAREs in IHC synaptic function has remained unresolved, and even questioned based on data obtained in organotypic cultures of organ of Corti explants derived from *Snap-25* null mice embryos. We here developed and characterized a *Snap-25* cKO mouse model in which the *Snap-25* gene is selectively inactivated in IHCs. Our results observed in the IHC subjected to SNAP-25 depletion before and after the hearing onset recapitulate several previous findings of *in vitro* studies using the total *Snap-25* KO. We found that, up to P8, the hearing organ of *Snap-25* cKO mice exhibited apparent normal hair cell organization, with no alterations to hair cell MET currents and normal ribbon synapse structure, as demonstrated by electrophysiological recordings, hair cell immunostaining and transmission electron microscopy. This suggests that the normal morpho-structural development of the organ of Corti and of the IHCs either does not require

SNAP-25, which would be consistent with what was reported in the CNS[23,36] or may occur with the residual pool of the SNAP-25 protein produced in the IHCs before total *Snap-25* depletion. However, during the second postnatal week of cochlear development, just before hearing onset, the IHCs of *Snap-25* cKO mice displayed a severe exocytotic defect affecting both the RRP and the SRP, which was associated with degeneration of ribbon synapses and hair cell loss. These results indicate that SNAP-25 is essential for the normal functioning and maintenance of IHC ribbon synapses. Consistent with these findings, synaptic disruption followed by neuronal death has been observed both *in vivo* and *in vitro* in the absence of several presynaptic proteins, including SNAP-25, VAMP, munc18 and syntaxin.[23,25,42–44] This neuronal loss was partly attributed to the implication of SNARE proteins in the release of neurotrophic factors such as BDNF, which is essential for synaptogenesis and neuronal survival.[38,45,46] However, the study of Zuccotti et al.[47] showed that the hearing function and hair cells survival were only moderately affected in BDNF conditional knockout mice, arguing against a major involvement of neurotrophins in the profound deafness we observed in the case of SNAP-25 inactivation.

One of the most notable findings of our study is the demonstration of the essential role played by SNAP-25 in the process of synaptic vesicle exocytosis in mature IHCs. This finding agrees well with the complete absence of evoked release in mature hippocampal cultures from total *Snap-25* KO mice.[34] We have also shown that the RRP exocytosis is severely affected first, suggesting the residual pool of the protein during *Snap-25* depletion is sufficient to ensure SRP release. This confirms a role for SNAP-25 in RRP fusion as observed in *Snap-25* KO embryonic chromaffin cells. Similarly to our observations in IHCs, the rapid phase of secretion has also been reported to be delayed in *Snap-25* KO embryonic chromaffin cells, which was rescued using viral transfer of *Snap-25*.[26,48,49] We also verified that the defects observed were, indeed, because of IHC *Snap-25* inactivation, by demonstrating that the AAV-mediated transfer of *Snap-25* cDNA to the inner ear of *Snap-25* cKO mice successfully rescued the fast component of IHC exocytosis, prevented the degeneration of both ribbon synapses and hair cells, and restored hearing function in the profoundly deaf *Snap-25* cKO mice. We hypothesized that the exocytotic defect derives first from the depletion of SNAP-25 at the synaptic hair cell active zone and that the degeneration of the ribbons is likely a consequence. Such statement agree well with previous reports showing ribbon degeneration occurring in IHCs wherein exocytosis is defective, such as in mice lacking otoferlin or after noise exposure and aging[11,50] or after noise exposure and aging.[27–30]

Our present results lead to the conclusion that SNAP-25 is essential for hearing function and provide strong evidence suggesting that protein is required to ensure synaptic exocytosis, maintenance of ribbon synapses and IHC survival.

### Limitations of the study

We provide *in vivo* evidence supporting the implication of SNAP-25 in synaptic exocytosis at both the immature and mature IHC ribbon synapse. There are two main limitations for this study: (1) We cannot state with certainty that our *in vivo* and *ex vivo* data reflect the function of IHC totally devoid of SNAP-25. Indeed, the kinetic of Cre expression *in vivo* and the half-life of SNAP-25 mRNAs and protein in IHC are challenging to determine. (2) In addition to its central role in synaptic exocytosis, SNAP-25 is involved in many other cellular processes such as cell development and survival. We therefore cannot exclude indirect and upstream membrane trafficking defects that might contribute to the observed impaired synaptic vesicle exocytosis in the IHCs in absence of SNAP-25.

## STAR★METHODS

Detailed methods are provided in the online version of this paper and include the following:

- KEY RESOURCES TABLE
- RESOURCE AVAILABILITY
  - Lead contact
  - Materials availability
  - Data and code availability
- EXPERIMENTAL MODEL AND SUBJECT DETAILS
  - Animals
- METHOD DETAILS
  - Genotyping

- ○ Deep sequencing of inner hair cell mRNA
- ○ RNAscope *in situ* hybridization
- ○ Recombinant AAV constructs
- ○ AAV delivery
- ○ Auditory brainstem responses (ABR) recording
- ○ Distortion product otoacoustic emission analysis
- ○ Immunofluorescence
- ○ Patch-clamp recording and capacitance measurement
- ○ Voltage stimulation
- ○ Intracellular $Ca^{2+}$ uncaging
- ○ Scanning electron microscopy
- ○ Transmission electron microscopy
- STATISTICAL ANALYSES

## SUPPLEMENTAL INFORMATION

Supplemental information can be found online at https://doi.org/10.1016/j.isci.2022.105628.

## ACKNOWLEDGMENTS

We thank Dr. Marie-José Lecomte for critical reading of the manuscript and all staff members of the Hearing Institute Bioimaging Core Facility of C2RT/C2RA for their excellent technical assistance. This work was supported by Fondation Pour l'Audition (FPA IDA05 to CP; FPA IDA03 to NM; FPA IDA08 to SS), DIM Ile de France (DIM Thérapie génique to CP and SS), EARGENCURE (ANR-17-CE18-0027 to SS), RHUAUDINNOVE (ANR-18-RHUS-0007 to CP and to SS).

## AUTHOR CONTRIBUTIONS

S.S., designed research and coordinated the project; CC., T.P., N.B., M.C., A.L., B.P., G.H., A.E., P.J., J.F., V.M., M.S., N.M., P.A., D.D., and S.S. performed research; S.S., C.C., D.D, and T.P. analyzed data; S.N. and M.S., contributed new reagents/analytic tools; J.B.D.M and C.P., reviewed the manuscript, C.C., D.D., and S.S. wrote the paper.

## DECLARATION OF INTERESTS

The authors declare no competing interests.

Received: March 10, 2022
Revised: August 24, 2022
Accepted: November 16, 2022
Published: December 22, 2022

## REFERENCES

1. Griesinger, C.B., Richards, C.D., and Ashmore, J.F. (2005). Fast vesicle replenishment allows indefatigable signalling at the first auditory synapse. Nature *435*, 212–215. https://doi.org/10.1038/nature03567.

2. Moser, T., and Beutner, D. (2000). Kinetics of exocytosis and endocytosis at the cochlear inner hair cell afferent synapse of the mouse. Proc. Natl. Acad. Sci. USA 97, 883–888.

3. Parsons, T.D., Lenzi, D., Almers, W., and Roberts, W.M. (1994). Calcium-triggered exocytosis and endocytosis in an isolated presynaptic cell: capacitance measurements in saccular hair cells. Neuron *13*, 875–883. https://doi.org/10.1016/0896-6273(94)90253-4.

4. Safieddine, S., El-Amraoui, A., and Petit, C. (2012). The auditory hair cell ribbon synapse: from assembly to function. Annu. Rev. Neurosci. *35*, 509–528. https://doi.org/10.1146/annurev-neuro-061010-113705.

5. Vincent, P.F.Y., Bouleau, Y., Charpentier, G., Emptoz, A., Safieddine, S., Petit, C., and Dulon, D. (2017). Different CaV1.3 channel isoforms control distinct components of the synaptic vesicle cycle in auditory inner hair cells. J. Neurosci. *37*, 2960–2975. https://doi.org/10.1523/JNEUROSCI.2374-16.2017.

6. Brandt, A., Striessnig, J., and Moser, T. (2003). CaV1.3 channels are essential for development and presynaptic activity of cochlear inner hair cells. J. Neurosci. *23*, 10832–10840. https://doi.org/10.1523/JNEUROSCI.23-34-10832.2003.

7. Platzer, J., Engel, J., Schrott-Fischer, A., Stephan, K., Bova, S., Chen, H., Zheng, H., and Striessnig, J. (2000). Congenital deafness and sinoatrial node dysfunction in mice lacking class D L-type Ca2+ channels. Cell *102*, 89–97. https://doi.org/10.1016/S0092-8674(00)00013-1.

8. Zampini, V., Johnson, S.L., Franz, C., Lawrence, N.D., Münkner, S., Engel, J., Knipper, M., Magistretti, J., Masetto, S., and Marcotti, W. (2010). Elementary properties of CaV1.3 Ca2+ channels expressed in mouse cochlear inner hair cells. J. Physiol. *588*, 187–199. https://doi.org/10.1113/jphysiol.2009.181917.

9. Beurg, M., Michalski, N., Safieddine, S., Bouleau, Y., Schneggenburger, R., Chapman, E.R., Petit, C., and Dulon, D. (2010). Control of exocytosis by synaptotagmins and otoferlin in auditory hair cells. J. Neurosci. *30*, 13281–13290. https://doi.org/10.1523/JNEUROSCI.2528-10.2010.

10. Michalski, N., Goutman, J.D., Auclair, S.M., Boutet de Monvel, J., Tertrais, M., Emptoz, A., Parrin, A., Nouaille, S., Guillon, M., Sachse, M., et al. (2017). Otoferlin acts as a Ca2+ sensor for vesicle fusion and vesicle pool replenishment at auditory hair cell ribbon synapses. Elife *6*, e31013. https://doi.org/10.7554/eLife.31013.

11. Roux, I., Safieddine, S., Nouvian, R., Grati, M., Simmler, M.-C., Bahloul, A., Perfettini, I., Le Gall, M., Rostaing, P., Hamard, G., et al. (2006). Otoferlin, defective in a human deafness form, is essential for exocytosis at the auditory ribbon synapse. Cell *127*, 277–289. https://doi.org/10.1016/j.cell.2006.08.040.

12. Frank, T., Rutherford, M.A., Strenzke, N., Neef, A., Pangršič, T., Khimich, D., Fejtova, A., Fetjova, A., Gundelfinger, E.D., Liberman, M.C., et al. (2010). Bassoon and the synaptic ribbon organize Ca2+ channels and vesicles to add release sites and promote refilling. Neuron *68*, 724–738. https://doi.org/10.1016/j.neuron.2010.10.027.

13. Jung, S., Oshima-Takago, T., Chakrabarti, R., Wong, A.B., Jing, Z., Yamanbaeva, G., Picher, M.M., Wojcik, S.M., Göttfert, F., Predoehl, F., et al. (2015). Rab3-interacting molecules 2α and 2β promote the abundance of voltage-gated CaV1.3 Ca2+ channels at hair cell active zones. Proc. Natl. Acad. Sci. USA *112*, E3141–E3149. https://doi.org/10.1073/pnas.1417207112.

14. Nouvian, R., Neef, J., Bulankina, A.V., Reisinger, E., Pangršič, T., Frank, T., Sikorra, S., Brose, N., Binz, T., and Moser, T. (2011). Exocytosis at the hair cell ribbon synapse apparently operates without neuronal SNARE proteins. Nat. Neurosci. *14*, 411–413. https://doi.org/10.1038/nn.2774.

15. Safieddine, S., and Wenthold, R. (1999). SNARE complex at the ribbon synapses of cochlear hair cells: analysis of synaptic vesicle- and synaptic membrane-associated proteins. Eur. J. Neurosci. *11*, 803–812.

16. Scheffer, D.I., Shen, J., Corey, D.P., and Chen, Z.-Y. (2015). Gene expression by mouse inner ear hair cells during development. J. Neurosci. *35*, 6366–6380. https://doi.org/10.1523/JNEUROSCI.5126-14.2015.

17. Uthaiah, R.C., and Hudspeth, A.J. (2010). Molecular anatomy of the hair cell's ribbon synapse. J. Neurosci. *30*, 12387–12399. https://doi.org/10.1523/JNEUROSCI.1014-10.2010.

18. Johnson, C.P., and Chapman, E.R. (2010). Otoferlin is a calcium sensor that directly regulates SNARE-mediated membrane fusion. J. Cell Biol. *191*, 187–197. https://doi.org/10.1083/jcb.201002089.

19. Ramakrishnan, N.A., Drescher, M.J., and Drescher, D.G. (2012). The SNARE complex in neuronal and sensory cells. Mol. Cell. Neurosci. *50*, 58–69. https://doi.org/10.1016/j.mcn.2012.03.009.

20. Verhage, M., and Sørensen, J.B. (2020). SNAREopathies: diversity in mechanisms and symptoms. Neuron *107*, 22–37. https://doi.org/10.1016/j.neuron.2020.05.036.

21. Glock, C., Heumüller, M., and Schuman, E.M. (2017). mRNA transport & local translation in neurons. Curr. Opin. Neurobiol. *45*, 169–177. https://doi.org/10.1016/j.conb.2017.05.005.

22. Caberlotto, E., Michel, V., Foucher, I., Bahloul, A., Goodyear, R.J., Pepermans, E., Michalski, N., Perfettini, I., Alegria-Prévot, O., Chardenoux, S., et al. (2011). Usher type 1G protein sans is a critical component of the tip-link complex, a structure controlling actin polymerization in stereocilia. Proc. Natl. Acad. Sci. USA *108*, 5825–5830. https://doi.org/10.1073/pnas.1017114108.

23. Washbourne, P., Thompson, P.M., Carta, M., Costa, E.T., Mathews, J.R., Lopez-Benditó, G., Molnár, Z., Becher, M.W., Valenzuela, C.F., Partridge, L.D., and Wilson, M.C. (2002). Genetic ablation of the t-SNARE SNAP-25 distinguishes mechanisms of neuroexocytosis. Nat. Neurosci. *5*, 19–26. https://doi.org/10.1038/nn783.

24. Roux, I., Hosie, S., Johnson, S.L., Bahloul, A., Cayet, N., Nouaille, S., Kros, C.J., Petit, C., and Safieddine, S. (2009). Myosin VI is required for the proper maturation and function of inner hair cell ribbon synapses. Hum. Mol. Genet. *18*, 4615–4628. https://doi.org/10.1093/hmg/ddp429.

25. Peng, L., Liu, H., Ruan, H., Tepp, W.H., Stoothoff, W.H., Brown, R.H., Johnson, E.A., Yao, W.-D., Zhang, S.-C., and Dong, M. (2013). Cytotoxicity of botulinum neurotoxins reveals a direct role of syntaxin 1 and SNAP-25 in neuron survival. Nat. Commun. *4*, 1472. https://doi.org/10.1038/ncomms2462.

26. Sørensen, J.B., Matti, U., Wei, S.-H., Nehring, R.B., Voets, T., Ashery, U., Binz, T., Neher, E., and Rettig, J. (2002). The SNARE protein SNAP-25 is linked to fast calcium triggering of exocytosis. Proc. Natl. Acad. Sci. USA *99*, 1627–1632. https://doi.org/10.1073/pnas.251673298.

27. Boero, L.E., Payne, S., Gómez-Casati, M.E., Rutherford, M.A., and Goutman, J.D. (2021). Noise exposure potentiates exocytosis from cochlear inner hair cells. Front. Synaptic Neurosci. *13*, 740368. https://doi.org/10.3389/fnsyn.2021.740368.

28. Chen, L., Han, M., Lu, Y., Chen, D., Sun, X., Yang, S., Sun, W., Yu, N., and Zhai, S. (2017). Molecular mechanisms underlying the protective effects of hydrogen-saturated saline on noise-induced hearing loss. Acta Otolaryngol. *137*, 1063–1068. https://doi.org/10.1080/00016489.2017.1328743.

29. Lepeta, K., Lourenco, M.V., Schweitzer, B.C., Martino Adami, P.V., Banerjee, P., Catuara-Solarz, S., de La Fuente Revenga, M., Guillem, A.M., Haidar, M., Ijomone, O.M., et al. (2016). Synaptopathies: synaptic dysfunction in neurological disorders - a review from students to students. J. Neurochem. *138*, 785–805. https://doi.org/10.1111/jnc.13713.

30. Peineau, T., Belleudy, S., Pietropaolo, S., Bouleau, Y., and Dulon, D. (2021). Synaptic release potentiation at aging auditory ribbon synapses. Front. Aging Neurosci. *13*, 756449. https://doi.org/10.3389/fnagi.2021.756449.

31. Sørensen, J.B., Nagy, G., Varoqueaux, F., Nehring, R.B., Brose, N., Wilson, M.C., and Neher, E. (2003). Differential control of the releasable vesicle pools by SNAP-25 splice variants and SNAP-23. Cell *114*, 75–86. https://doi.org/10.1016/S0092-8674(03)00477-X.

32. Schiavo, G., Benfenati, F., Poulain, B., Rossetto, O., Polverino de Laureto, P., DasGupta, B.R., and Montecucco, C. (1992). Tetanus and botulinum-B neurotoxins block neurotransmitter release by proteolytic cleavage of synaptobrevin. Nature *359*, 832–835. https://doi.org/10.1038/359832a0.

33. Söllner, T., Whiteheart, S.W., Brunner, M., Erdjument-Bromage, H., Geromanos, S., Tempst, P., and Rothman, J.E. (1993). SNAP receptors implicated in vesicle targeting and fusion. Nature *362*, 318–324. https://doi.org/10.1038/362318a0.

34. Bronk, P., Deák, F., Wilson, M.C., Liu, X., Südhof, T.C., and Kavalali, E.T. (2007). Differential effects of SNAP-25 deletion on Ca2+ -dependent and Ca2+ -independent neurotransmission. J. Neurophysiol. *98*, 794–806. https://doi.org/10.1152/jn.00226.2007.

35. Delgado-Martínez, I., Nehring, R.B., and Sørensen, J.B. (2007). Differential abilities of SNAP-25 homologs to support neuronal function. J. Neurosci. *27*, 9380–9391. https://doi.org/10.1523/JNEUROSCI.5092-06.2007.

36. Hoerder-Suabedissen, A., Korrell, K.V., Hayashi, S., Jeans, A., Ramirez, D.M.O., Grant, E., Christian, H.C., Kavalali, E.T., Wilson, M.C., and Molnár, Z. (2019). Cell-specific loss of SNAP25 from cortical projection neurons allows normal development but causes subsequent neurodegeneration. Cereb. Cortex *29*, 2148–2159. https://doi.org/10.1093/cercor/bhy127.

37. Kádková, A., Radecke, J., and Sørensen, J.B. (2019). The SNAP-25 protein family. Neuroscience *420*, 50–71. https://doi.org/10.1016/j.neuroscience.2018.09.020.

38. Shimojo, M., Courchet, J., Pieraut, S., Torabi-Rander, N., Sando, R., Polleux, F., and Maximov, A. (2015). SNAREs controlling vesicular release of BDNF and development of callosal axons. Cell Rep. *11*, 1054–1066. https://doi.org/10.1016/j.celrep.2015.04.032.

39. Yang, H., Zhang, M., Shi, J., Zhou, Y., Wan, Z., Wang, Y., Wan, Y., Li, J., Wang, Z., and Fei, J. (2017). Brain-specific SNAP-25 deletion leads to elevated extracellular glutamate level and schizophrenia-like behavior in mice. Neural Plast. *2017*, 4526417. https://doi.org/10.1155/2017/4526417.

40. de Wit, J., Toonen, R.F., and Verhage, M. (2009). Matrix-dependent local retention of secretory vesicle cargo in cortical neurons. J. Neurosci. *29*, 23–37. https://doi.org/10.1523/JNEUROSCI.3931-08.2009.

41. Südhof, T.C., and Rothman, J.E. (2009). Membrane fusion: grappling with SNARE and SM proteins. Science *323*, 474–477. https://doi.org/10.1126/science.1161748.

42. Berliocchi, L., Fava, E., Leist, M., Horvat, V., Dinsdale, D., Read, D., and Nicotera, P. (2005). Botulinum neurotoxin C initiates two different programs for neurite degeneration and neuronal apoptosis. J. Cell Biol. *168*, 607–618. https://doi.org/10.1083/jcb.200406126.

43. Vardar, G., Chang, S., Arancillo, M., Wu, Y.-J., Trimbuch, T., and Rosenmund, C. (2016). Distinct functions of syntaxin-1 in neuronal maintenance, synaptic vesicle docking, and fusion in mouse neurons. J. Neurosci. *36*, 7911–7924. https://doi.org/10.1523/JNEUROSCI.1314-16.2016.

44. Verhage, M., Maia, A.S., Plomp, J.J., Brussaard, A.B., Heeroma, J.H., Vermeer, H., Toonen, R.F., Hammer, R.E., van den Berg, T.K., Missler, M., et al. (2000). Synaptic assembly of the brain in the absence of neurotransmitter secretion. Science *287*, 864–869. https://doi.org/10.1126/science.287.5454.864.

45. Arora, S., Saarloos, I., Kooistra, R., van de Bospoort, R., Verhage, M., and Toonen, R.F. (2017). SNAP-25 gene family members differentially support secretory vesicle fusion. J. Cell Sci. *130*, 1877–1889. https://doi.org/10.1242/jcs.201889.

46. Puntman, D.C., Arora, S., Farina, M., Toonen, R.F., and Verhage, M. (2021). Munc18-1 is essential for neuropeptide secretion in neurons. J. Neurosci. *41*, 5980–5993. https://doi.org/10.1523/JNEUROSCI.3150-20.2021.

47. Zuccotti, A., Kuhn, S., Johnson, S.L., Franz, C., Singer, W., Hecker, D., Geisler, H.-S., Köpschall, I., Rohbock, K., Gutsche, K., et al. (2012). Lack of brain-derived neurotrophic factor hampers inner hair cell synapse physiology, but protects against noise-induced hearing loss. J. Neurosci. *32*, 8545–8553. https://doi.org/10.1523/JNEUROSCI.1247-12.2012.

48. Criado, M., Gil, A., Viniegra, S., and Gutiérrez, L.M. (1999). A single amino acid near the C terminus of the synaptosomeassociated protein of 25 kDa (SNAP-25) is essential for exocytosis in chromaffin cells. Proc. Natl. Acad. Sci. USA *96*, 7256–7261. https://doi.org/10.1073/pnas.96.13.7256.

49. Wei, S., Xu, T., Ashery, U., Kollewe, A., Matti, U., Antonin, W., Rettig, J., and Neher, E. (2000). Exocytotic mechanism studied by truncated and zero layer mutants of the C-terminus of SNAP-25. EMBO J. *19*, 1279–1289. https://doi.org/10.1093/emboj/19.6.1279.

50. Stalmann, U., Franke, A.J., Al-Moyed, H., Strenzke, N., and Reisinger, E. (2021). Otoferlin is required for proper synapse maturation and for maintenance of inner and outer hair cells in mouse models for DFNB9. Front. Cell. Neurosci. *15*, 677543. https://doi.org/10.3389/fncel.2021.677543.

51. Tang, F., Barbacioru, C., Wang, Y., Nordman, E., Lee, C., Xu, N., Wang, X., Bodeau, J., Tuch, B.B., Siddiqui, A., et al. (2009). mRNA-Seq whole-transcriptome analysis of a single cell. Nat. Methods *6*, 377–382. https://doi.org/10.1038/nmeth.1315.

52. Tang, F., Barbacioru, C., Bao, S., Lee, C., Nordman, E., Wang, X., Lao, K., and Surani, M.A. (2010). Tracing the derivation of embryonic stem cells from the inner cell mass by single-cell RNA-seq analysis. Cell Stem Cell *6*, 468–478. https://doi.org/10.1016/j.stem.2010.03.015.

53. Michalski, N., Michel, V., Caberlotto, E., Lefèvre, G.M., van Aken, A.F.J., Tinevez, J.-Y., Bizard, E., Houbron, C., Weil, D., Hardelin, J.-P., et al. (2009). Harmonin-b, an actin-binding scaffold protein, is involved in the adaptation of mechanoelectrical transduction by sensory hair cells. Pflugers Arch. *459*, 115–130. https://doi.org/10.1007/s00424-009-0711-x.

54. Vincent, P.F.Y., Bouleau, Y., Safieddine, S., Petit, C., and Dulon, D. (2014). Exocytotic machineries of vestibular type I and cochlear ribbon synapses display similar intrinsic otoferlin-dependent Ca2+ sensitivity but a different coupling to Ca2+ channels. J. Neurosci. *34*, 10853–10869. https://doi.org/10.1523/JNEUROSCI.0947-14.2014.

## STAR★METHODS

### KEY RESOURCES TABLE

| REAGENT or RESOURCE | SOURCE | IDENTIFIER |
|---|---|---|
| **Antibodies** | | |
| Chicken polyclonal anti-GFP | Abcam | Cat#13970; RRID:AB_300798 |
| Rabbit polyclonal anti-Otoferlin | Roux et al., 2006 | N/A |
| Mouse monoclonal anti-CtBP2 | Fisher scientific | Cat#612044; RRID:AB_399431 |
| Rabbit polyclonal anti-Ribeye | SYSY | Cat#192–103; RRID:AB_2086775 |
| Guinea pig polyclonal anti-Ribeye | SYSY | Cat#192104; RRID:AB_2800537 |
| Mouse monoclonal anti-GluR2 | Sigma-Aldrich | Cat#MAB397; RRID:AB_11212990 |
| Rabbit polyclonal anti-myo6 | Roux et al., 2009 | N/A |
| Rabbit polyclonal anti-myo7A | Proteus Blosciences | Cat#25–6790; RRID:AB_10015251 |
| Chicken polyclonal anti-neurofilament | Sigma-Aldrich | Cat#AB5539; RRID:AB_11212161 |
| Goat Anti-Rabbit-IgG - Atto 647N | Sigma-Aldrich | Cat#40839; RRID:AB_1137669 |
| Goat Anti-Rabbit IgG - Atto 488 | Sigma-Aldrich | Cat#18772; RRID:AB_1137637 |
| Goat Anti-Mouse IgG - Atto 633 | Sigma-Aldrich | Cat#78102; RRID:AB_1137635 |
| Alexa Fluor® 488 conjugated Goat Anti-Guinea pig IgG | Abcam | Cat#ab150185; RRID:AB_2736871 |
| Goat Anti-Mouse IgG - Atto 550 | Sigma-Aldrich | Cat#43314; RRID:AB_1137651 |
| Goat anti-rabbit IgG - Alexa fluor 488 | Sigma-Aldrich | Cat# A32731; RRID:AB_2633280 |
| Goat anti-chicken IgG – Alexa 488 | Sigma-Aldrich | Cat#A11039; RRID:AB_2534096 |
| **Bacterial and virus strains** | | |
| AAV8-CMV-PI-SNAP-25 | This article | N/A |
| AAV8.CMV.HI.eGFPCre.WPRE.SV40 | Addgene | Cat#105545 |
| **Chemicals, peptides, and recombinant proteins** | | |
| SuperScript III Reverse Transcriptase | Thermo Fisher Scientific | Cat# 18080044 |
| 3M Vetbond glue | Phymep | Cat#1469SB |
| Paraformaldehyde | Electron Microscopy Science | Cat#15714 |
| Horse serum | Thermo Fisher Scientific | Cat#16050122 |
| Triton X-100 | Sigma-Aldrich | Cat#X-100 |
| DAPI | Sigma-Aldrich | Cat#MBD0015 |
| FluorSaveTM | Calbiochem | Cat#345789 |
| ProLong Gold Antifade Mountant | Invitrogen | Cat#P10144 |
| Cesium chloride | Sigma-Aldrich | Cat# 289329–25G |
| Magnesium chloride hexahydrate | Sigma-Aldrich | Cat# M2670-500G |
| HEPES | Sigma-Aldrich | Cat# H3375-100G |
| Ethylene glycol-bis(2-aminoethylether)-N,N,N0,N0-tetraacetic acid | Sigma-Aldrich | Cat# E4378-10G |
| Adenosine 5′-triphosphate magnesium salt | Sigma-Aldrich | Cat# A9187-500MG |
| Guanosine 5′-triphosphate sodium salt hydrate | Sigma-Aldrich | Cat# G8877-100MG |
| Tetraethylammonium chloride | Sigma-Aldrich | Cat# T2265-25G |
| Calcium chloride | Sigma-Aldrich | Cat# C5080-500G |
| Xylazine (Rompun 2%) | Centravet | Cat#ROM001 |
| Ketamine (Imalgene 1000) | Centravet | Cat# IMA004 |
| DM-nitrophen | Interchim | Cat#FP-005460 |

(*Continued on next page*)

*Continued*

| REAGENT or RESOURCE | SOURCE | IDENTIFIER |
|---|---|---|
| Glutaraldehyde | Electron Microscopy Science | CAS #111-30-8 |
| Osmium tetraoxide | Electron Microscopy Science | CAS #20816-12-0 |
| Thiocarbohydrazide | Electron Microscopy Science | CAS #2231-57-4 |
| Hexamethyldisilazane | Sigma-Aldrich | Cat#40191–100ML |
| Spurr's low-viscosity epoxy resin | Electron Microscopy Science | Cat#14310 |
| Uranyl acetate | Electron Microscopy Science | Cat#22400 |
| Lead citrate | Electron Microscopy Science | Cat#17800 |
| **Critical commercial assays** | | |
| RNAscope Multiplex Fluorescent Reagent Kit v2 Assay | Advanced Cell Diagnostics | Cat#323100 |
| Mm-Snap-25 | Advanced Cell Diagnostics | Cat#16471 |
| Opal dye 570 fluorophore | Akoya Biosciences | Cat#FP1488001KT |
| **Experimental models: Organisms/strains** | | |
| Mouse : Snap-25$^{lox/lox}$: C57BL/6N | This paper | N/A |
| Mouse: Ai9(Rosa26-CAG-loxP-stop-loxP-tdTomato) | Jackson laboratories | #007914 |
| Mouse : PMyo15-hcre$^{+/KI}$: C57BL/6 N | Carbelotto et al.[22] | N/A |
| Mouse : C57BL/6J mice producing Flp recombinase | Carbelotto et al.[22] | N/A |
| Mouse: Snap-25 cKO: C57BL/6N | This paper | N/A |
| **Oligonucleotides** | | |
| 5′-GAAATCTCTGTAATGACTTGAGGACCC-3′ | This paper | Primer-1 (reverse) |
| 5′-CCTCCATCTACCAAATGTTGAAGAGC-3′ | This paper | Primer-2 (forward) |
| 5′-AGGGACCTGACTCCACTTTGGG-3′ | This paper | Primer-3 (forward) |
| 5′-GGAACTGACCTTTCTTAGAGATCTTGGG-3′ | This paper | Primer-4 (reverse) |
| 5′-TGGTGCACAGTCAGCAGGTTGG-3′ | This paper | Primer-5 (reverse) |
| **Recombinant DNA** | | |
| AAV.CMV.PI.EGFP.WPRE.bGH | Addgene | Cat#105530 |
| pAAV.CMV-PI-SNAP-25 | This paper | N/A |
| **Software and algorithms** | | |
| ImageJ | Wayne Rasband, National Institutes of Health | https://imagej.nih.gov/ij/ |
| GraphPad Prism | GraphPad Software | https://www.graphpad.com/scientificsoftware/prism/ |
| Adobe Photoshop CS6 | Adobe | https://www.adobe.com/ |
| Matlab | MathWorks | https://fr.mathworks.com/ |
| RT-Lab | Echodia | http://echodia.fr |
| Patchmaster | HEKA Electronic | RRID:SCR_000034 |
| OriginPro | OriginLab | RRID: SCR_015636 |
| analySIS | Soft Imaging System | RRID: SCR_015636 |
| **Other** | | |
| Single capillary (intracochear injection) | World Precision Instruments | Cat#1B150-4 |

## RESOURCE AVAILABILITY

### Lead contact

Further information and request for resources and reagents should be directed to and will be fulfilled by the lead contact, Saaid Safieddine (saaid.safieddine@pasteur.fr).

### Materials availability

All reagents and mouse lines generated in this study are available from the lead contact.

### Data and code availability

All data reported in this paper is available from the lead contact upon request. Of note, deep sequencing data we provide here concerns only the neuronal SNAREs and proteins essential for IHC synaptic transmission, which is the scope of the article. These data represent only a small fraction of a bigger deep sequencing dataset that is currently being analyzed and will be the subject of a separate publication.

This paper does not report original code.

Any additional information required to reanalyze the data reported in this work paper is available from the lead contact upon request.

## EXPERIMENTAL MODEL AND SUBJECT DETAILS

### Animals

The *Snap-25*$^{lox/lox}$ (MGI:98331) mice were generated by homologous recombination (Institut Pasteur and Clinique de la Souris, Illkirch, France). A targeting vector was designed in which loxP sites were introduced upstream and downstream of *Snap-25* exon 4, and a neo cassette flanked with Frt sites as selectable marker was introduced downstream of exon 4. The targeting construct was electroporated into embryonic stem cells from the C57BL6/N mouse strain, and 4 positive ES cells were selected. Stem cells carrying the targeted construct were injected into blastocysts from C57BL/6N mice. After germline transmission, mice were crossed with C57BL/6J mice producing Flp recombinase to remove the neo cassette. The *Snap-25*$^{\mathrm{lox/lox}}$ mice lack the neo cassette and behave like wild-type mice. *Snap-25*$^{\mathrm{lox/lox}}$ mice were crossed either with Myo15-cre recombinant mice carrying the Cre recombinase gene driven by the myosin-15 gene promoter which, in the inner ear, deletes only the floxed fragment in hair cells[22] or subjected to intracochlear injection of AAV8-CMV-GFP-Cre at different time points.

The *Rosa*-tdTomato mice were obtained from Jackson Laboratories.

Male and female mice were used in this study and housed in a temperature-controlled room and maintained on a 12/12 h light/dark cycle. Food and water were available *ad libitum* and experiments were conducted according to the European guide for the care and use of laboratory animals and approved by the ethics committee of Institut Pasteur under the APAFIS #18368–019010910106739 (France).

## METHOD DETAILS

### Genotyping

Genotyping of *Snap-25*$^{\mathrm{lox/lox}}$ recombinant animals was carried out by means of two PCR amplifications, using primer-1 and primer 2 to detect the wild-type allele (1071-bp amplicon), floxed allele (1256-bp amplicon), and deleted allele lacking *Snap-25* exon 4 (274-bp amplicon). Genotyping of *Snap-25*$^{\mathrm{lox/lox}}$/PMyo15-hCre (Snap-25 cKO) animals was carried out using two additional PCR amplifications. Primer-3 and primer-4 to detect the presence of the wild-type (587 bp amplicon) allele. Primer-3 and Primer-5 were used to detect the presence of the Cre allele (500 bp amplicon) leading the *Snap-25* exon 4 deletion in the inner ear hair cells. The list of primers and sequences used for genotyping can be found in the key resources table.

### Deep sequencing of inner hair cell mRNA

IHC samples were collected in triplicate from excised organs of Corti (from P2, P7 and P16 mice) placed under two nylon meshes and observed with an Olympus 40X water-immersion objective (Tokyo, Japan). A strong positive pressure was applied through a patch pipette containing Hank's balanced salt solution to separate IHCs from the neighboring supporting cells. A second patch pipette containing $\sim$2 $\mu$L of Hank's solution was used to collect 20 IHCs. Each sample consisted in 20 IHCs collected from a different organ of Corti. The sampled IHCs were then processed for reverse transcription to generate cDNA from mRNA, the PCR amplification of cDNAs, and deep-sequencing as described elsewhere.[51,52] Briefly, sampled IHCs were placed in a tube containing the SuperScript III Reverse Transcriptase reagents, wherein the mRNA was reverse-transcribed to generate cDNA, using a poly(T) primer with an anchor sequence (UP1). A poly(A) tail was added to the 3′ end of the first-strand cDNAs, and the second-strand cDNAs were then synthesized with poly(T) primers with another anchor sequence (UP2). The cDNAs were then uniformly amplified by PCR with primers targeting the UP1 and UP2 anchor sequences. The PCR products were purified, and samples were deep-sequenced with an Illumina Version 3 sequencer (100 bp paired-end reads, Eurofins, Germany). For each transcript, the reads were mapped onto the mouse genome (Genomatix, Munich, Germany) and normalized expression values were calculated as follows: $f = 10^7 \times (\#reads_{region})/(\#reads_{mapped})$, where $10^7$ is a normalization constant, $\#reads_{region}$ the number of reads (sum of base pairs) corresponding to the transcript, and $\#reads_{mapped}$ the total number of mapped reads in the sample (sum of base pairs). We did not normalize by the length of the sequenced mRNA because the vast majority of sequenced reads were located at the 3′ end of mRNAs, next to the poly(A) tail. We considered only unambiguous unique hits for the analysis.

### RNAscope *in situ* hybridization

The cochleae were extracted in a cold PBS solution and then fixed in 4% PFA for 1 h at room temperature. The organs were decalcified in 0.35 M EDTA, pH 7.5 at room temperature for 2 h. The bone of the cochleae was removed by microdissection and then fixed in 4% PFA for 45 min. For RNA *in situ* hybridization, we used the RNAscope kit (RNAscope Multiplex Fluorescent Reagent Kit v2 Assay) according to the manufacturer's instructions. In brief, the organs were dehydrated in successive ethanol washes, then dried 10 min at room temperature. After incubation with hydrogen peroxyde for 10 min at room temperature, followed by Protease Plus treatment at 40°C for 30 min, the tissues were hybridized with the appropriate target probe (Mm-Snap-25-C1) at 40°C for 2 h. This was followed by four successive amplification steps using *Amp1*, *Amp2*, *Amp3*, and horserasish peroxidase. The Opal dye 570 fluorescent probe at 1/1000 dilution was then added to label the channel C1. Coverslips were mounted with Prolong Gold. channel C1. For RNAscope spot counting, 3D-stacks with an interval of 0.25 μm were analyzed using the Imaris software (v9.9, Bitplane). The spots were subjectively selected by thresholding the quality of a 3D Gaussian fitting, including or excluding spots.

### Recombinant AAV constructs

The coding sequence of the murine *Snap-25* cDNA (NM_011428.3) was inserted into p0101 (pAAV.CMV.PI.EGFP.WPRE.bGH) plasmid from Addgene in place of eGFP. The recombinant vector AAV2-CMV-PI-SNAP-25 was packaged in the AAV8 capsid and produced by the Penn Vector Core facility with a titer of $1.72 \times 10^{14}$ GC/mL. The cochlear delivery of the Cre recombinase was carried out using the rAAV construct from Addgene containing the inverted terminal repeat of AAV2 and the capsid of AAV8 serotypes with CMV driven eGFP-Cre (AAV8.CMV.HI.eGFP-Cre.WPRE.SV40) with a titer of $2.88 \times 10^{13}$ GC/mL.

### AAV delivery

The protocols were approved by the Animal Care and Use Committee of the Institut Pasteur. Isoflurane anesthesia was used on P1-P3 and P12-P15 mice and animals were placed on a warming pad. For P1-P3 mice a local injection of lidocaine 2% (5 mg/kg) was performed under the skin before opening. For P12-P15 mice, local injection of lidocaine 2% was combined to a meloxicam (1 mg/kg) subcutaneous injection 30 min before surgery. Animals were shaved (P12-P15) and the skin disinfected using betadine, the eyes were protected with ocry-gel. A left postauricular incision was made, and the cochlear basal turn, stapedial artery and facial nerve were used as landmarks to access the round window membrane of P1-P3 mice. For P12-P15 mice, the otic bulla was exposed and opened to access the round window membrane. A micropipette (10 μm diameter) was used to inject 1 to 2 μL of AAV viral vectors through the round window membrane. The hole was then plugged with muscle and connective tissue, and the skin was sealed with biological glue (3M Vetbond). Mice were kept on a warming pad until they woke up and then placed into their home cage.

### Auditory brainstem responses (ABR) recording

The mice were anesthetized with ketamine (100 mg/kg) and xylazine (10 mg/kg) and placed on a warming pad into an attenuated-sound box. Three electrodes were placed on the vertex, the ipsilateral mastoid, and the lower back as the ground electrode. Pure-tone stimuli were used at frequencies of 5, 10, 15, 20, 32, and 40 kHz. Sound intensities of 10 to 110 dB, in 10-dB steps, were tested. The hearing threshold was determined as the lowest stimulus level resulting in a visual recognition of ABR waves. ABR analysis was performed with Matlab software. The amplitude of ABR wave I was measured (Matlab) for sounds of high intensity (70 to 90 dB). Mice were kept on a warming pad until they woke up and then placed into their home cage.

### Distortion product otoacoustic emission analysis

Distortion product otoacoustic emissions (DPOAEs) were measured to evaluate OHC function. Mice were anesthetized with ketamine and xylazine as previously described, and body temperature was maintained close to 37°C with a warming pad. DPOAEs were conducted with Otophylab (Echodia) and analyzed with RT-Lab software or with CubeDis system, Mimosa Acoustics, ER10B microphone, Etymotic Research. The DPOAE at a frequency 2*f1-f2* was recorded in response to two simultaneously presented primary tones of equal energy levels and distinct frequencies *f1* and *f2*, with *f2/f1* = 1.20. Frequency *f2* was swept at 12 kHz and 16 kHz or 10 kHz and 15 kHz and responses were recorded in response to a 80 dB SPL stimulation. The DPOAE threshold was plotted against frequency *f2*. The DPOAE threshold was defined as the smallest primary level leading to a detectable DPOAE.

### Immunofluorescence

The cochleas were dislodged from the skulls of mutant*Snap-25* cKO, or Cre-injected *Snap-25*$^{lox/lox}$ mice and from control non-injected *Snap-25*$^{lox/lox}$, or wild-type C57BL6/J mice depending on experiments. They were perfused with 4% paraformaldehyde in PBS for 45 min at room temperature. The organs of Corti were microdissected free from the rest of the cochlea and whole mounts of sensory epithelium were rinsed (3 × 10 min) with PBS and incubated for 1 h at room temperature in PBS supplemented with 20% normal horse serum and 0.3% Triton X-100.

The samples were then incubated overnight with various primary antibodies in PBS: chicken anti-GFP (1:500), rabbit anti-otoferlin (1:200), mouse anti-CTBP2 (1:100), guinea pig anti-ribeye (1:700), rabbit anti-ribeye (1:200), mouse anti-GluA2 (1:2000), Myosin 7a (1:700), and/or rabbit anti-myosin 6 (1:200)).

The samples were rinsed with (3 × 10 min) PBS and incubated for 1 h with various solutions of secondary antibodies (1:500 dilution): ATTO-647–conjugated goat anti-rabbit IgG antibody, Alexa-488–conjugated goat anti-chicken IgG antibody, Alexa-488 goat anti-rabbit IgG antibody, ATTO-488 goat anti-rabbit IgG antibody, Alexa-488 goat anti-guinea pig IgG, ATTO 633-conjugated goat anti-mouse IgG antibody, and ATTO-550–conjugated goat anti-mouse IgG antibody. Nuclei were labeled by incubation with 4′,6-diamidino-2-phenylindole (DAPI) (1:7500) for 10 min. The samples were rinsed with (3 × 10 min) PBS and then mounted in Fluorsave medium.

For immunofluorescent stainings after RNAscope IHS, the tissues were incubated in a blocking solution (0.3% triton, 1% BSA, 20% goat serum) 1 h at room temperature, and then incubated overnight at room temperature with the primary antibody (rabbit-antibody directed against Myosin 7a (1:200)), followed by 2 h of incubation with the secondary antibody (goat anti-rabbit alexa fluor 488 (1:500)) at room temperature. DAPI was finally added at 1:1000 concentration during 10 min at room temperature. The tissues were mounted on coverslip with ProLong Gold Antifade Mountant. The list of antibodies used can be found in the key resources table.

Images were captured with Zeiss LSM-700 or LSM-900 confocal microscopes equipped with a Plan Apochromat 63x/1.4 N.A. oil immersion lens (Carl Zeiss).

### Patch-clamp recording and capacitance measurement

Electrophysiological whole-cell patch-clamp recordings of hair cell mechanoelectrical transduction currents were performed in cochlear explants from P8 mice, as previously described.[53]

All the recordings of IHC capacitance measurement were performed at the mid-apical region of the cochlea 20–40% normalized distance from the apex, an area encoding frequencies ranging from 8 to 16 kHz, with an EPC10 amplifier controlled by Patchmaster software. For AAV8-GFP-Cre, only GFP-expressing IHCs were recorded. IHCs were otherwise selected for recording at random from the tissue preparation. Patch pipettes were pulled with a micropipette puller (P-97 Flaming/Brown; Sutter Instrument) and fire-polished with an MF-830 microforge (Narishige) to obtain a resistance range of 2 to 4 MΩ. Patch pipettes were filled with an intracellular cesium-based solution containing the following: 145 mM CsCl, 1 mM $MgCl_2$, 5 mM HEPES, 1 mM EGTA, 20 mM tetraethylammonium chloride, 2 mM ATP, and 0.3 mM GTP, pH 7.2, 300 mOsm. Changes in cell membrane capacitance ($\Delta C_m$) were used to monitor the fusion of synaptic vesicles during exocytosis. $\Delta C_m$ was measured with the Lindau and Neher (1988) technique, using the lock-in amplifier Patchmaster software (HEKA) and applying a 1 kHz command sine wave (20 mV amplitude) at a holding potential of −80 mV before and after the pulse experiment. As recording conditions can greatly influence capacitance measurements, only IHC patch-clamp recordings with low series resistance, below 10 MΩ, and a maximum leak current of 25 pA (at $V_h$ = −80 mV) were considered in this study.

### Voltage stimulation

Two different protocols were used. First, readily releasable pool (RRP) exocytosis was recorded by the depolarization of IHCs from −80 to −10 mV for increasing durations, from 5 to 80 ms, in 5 ms increments. Second, the replenishment in vesicles of the synaptic zone was probed by depolarizing IHCs during a train of 100 ms pulses from −80 to −10 mV.

### Intracellular $Ca^{2+}$ uncaging

We triggered a rapid increase in intracellular $Ca^{2+}$ concentration from the caged $Ca^{2+}$ chelator DM-Nitrophen, using a brief (100 ms) flash from a 365 nm UV light source delivered by a Mic-LED-365 (350 mW; Prizmatix). The UV LED was connected directly to the epi-illumination port at the rear of a Nikon FN1 upright microscope and illumination was focused through the 60× objective (CFI Fluor 60x W NIR, WD = 2.0 mm, NA = 1). HCs were loaded with 145 mM CsCl, 5 mM HEPES, 20 mM TEA, 10 mM DM-Nitrophen, and 10 mM $CaCl_2$. Following patch rupture, we systematically waited for 2 min at a holding potential of −70 mV to load and equilibrate the cells with the intrapipette solution. Upon UV photolysis, $[Ca^{2+}]_i$, continuously measured with a C2 confocal system and NIS-Elements imaging software (Nikon) coupled to the FN1 microscope, reached a peak of 20 ± 5 μM within 15–20 ms.[54]

### Scanning electron microscopy

Inner ears were fixed by incubation in 2.5% glutaraldehyde in 0.1 M phosphate buffer (pH 7.3) for 2 h at room temperature. The organs of Corti were microdissected and the samples were incubated in an alternating series of solutions of 1% osmium tetroxide (O) and 0.1 M thiocarbohydrazide (T) (sequence: OTOTO). The samples were then dehydrated by incubation in a graduated series of ethanol solutions and dried to critical point with hexamethyldisilazane. Samples were analyzed with a Jeol JSM6700F-type field emission scanning electron microscope operating at 5 kV. Images were obtained with a charge-coupled camera (SIS Megaview3; Surface Imaging Systems), acquired with analySIS (Soft Imaging System), and processed with Photoshop CS6.

### Transmission electron microscopy

Cochleas were perfused with 4% paraformaldehyde and 2% glutaraldehyde in Sorensen buffer at pH 7.4 and immersed in the fixative solution for 2 h. They were then postfixed by incubation overnight in 1% osmium tetraoxide in cacodylate buffer at 4°C. They were dehydrated in a graded series of acetone concentrations and embedded in Spurr's low-viscosity epoxy resin, which was then hardened at 70°C. We cut 70 nm sections of the sensory epithelium (organ of Corti) and collected them on 100-mesh parallel-bar copper grids. The grids were contrast-stained with 4% uranyl acetate in $dH_2O$ for 40 min and then with Reynold's lead citrate for 3 min. The sections were viewed in a FEI *Tecnai* G2 *200 kV* transmission electron microscope.

## STATISTICAL ANALYSES

All statistical analyses were performed in GraphPad and the following tests were used, as appropriate, depending on the data concerned: Mann-Whitney test, Student's *t* test, one-way ANOVA, two-way ANOVA. Statistical significance is indicated in the figures as follows: n.s., not significant; *$p< 0.05$; **$p< 0.01$; ***$p< 0.001$, ****$p< 0.0001$. For ABRs, DPOAEs, and ribbon counts, all values are given as means ± standard deviation. For IHC patch-clamp recordings and $Ca^{2+}$ imaging, values are given as means ± SEM.